

GMS-VINS: Multi-category Dynamic Objects Semantic Segmentation for Enhanced Visual-Inertial Odometry Using a Promptable Foundation Model

Rui Zhou¹, Jingbin Liu^{2*}, Junbin Xie¹, Jianyu Zhang¹, Yingze Hu¹ and Jiele Zhao¹

¹Electronic Information School, Wuhan University

²State Key Laboratory of Information Engineering in Surveying, Mapping and Remote Sensing, Wuhan University

Abstract—Visual-inertial odometry (VIO) is widely used in various fields, such as robots, drones, and autonomous vehicles, due to its low cost and complementary sensors. Most VIO methods presuppose that observed objects are static and time-invariant. However, real-world scenes often feature dynamic objects, compromising the accuracy of pose estimation. These moving entities include cars, trucks, buses, motorcycles, and pedestrians. The diversity and partial occlusion of these objects present a tough challenge for existing dynamic object removal techniques. To tackle this challenge, we introduce GMS-VINS, which integrates an enhanced SORT algorithm along with a robust multi-category segmentation framework into VIO, thereby improving pose estimation accuracy in environments with diverse dynamic objects and frequent occlusions. Leveraging the promptable foundation model, our solution efficiently tracks and segments a wide range of object categories. The enhanced SORT algorithm significantly improves the reliability of tracking multiple dynamic objects, especially in urban settings with partial occlusions or swift movements. We evaluated our proposed method using multiple public datasets representing various scenes, as well as in a real-world scenario involving diverse dynamic objects. The experimental results demonstrate that our proposed method performs impressively in multiple scenarios, outperforming other state-of-the-art methods. This highlights its remarkable generalization and adaptability in diverse dynamic environments, showcasing its potential to handle various dynamic objects in practical applications.

Index Terms—Visual-Inertial Odometry, Visual Localization, Mobile Mapping, Positioning, Semantic Segmentation

I. INTRODUCTION

Accurate motion estimation in unfamiliar scenarios is crucial for various vision and robotics applications, including augmented reality (AR), unmanned aerial vehicles (UAVs) and autonomous driving. Techniques like visual-inertial SLAM (VI-SLAM) and visual-inertial odometry (VIO) [1] are broadly employed in this domain, serving as fundamental methods for numerous robotic applications that demand accurate positioning or navigation in environments where GNSS (Global Navigation Satellite System) signals are obstructed.

Most current visual SLAM and VIO methods typically presume that observed objects remain static and time-invariant. However, as a robot navigates in urban environments, moving objects like pedestrians and vehicle can adversely affect the precision of VIO system localization, causing a mismatch

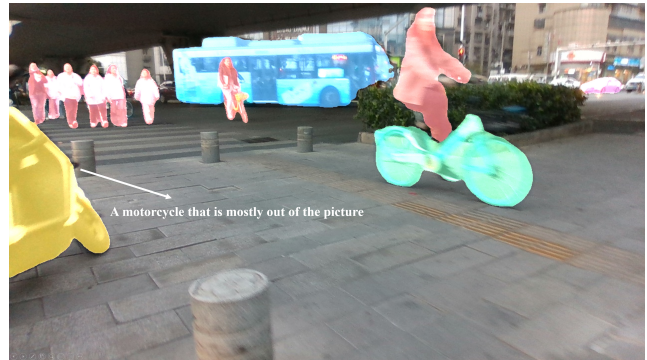


Fig. 1: Our Method, GMS-VINS, in real-world urban environments with diverse moving objects. Our method effectively segments various moving objects even under conditions of partial occlusion, demonstrating the efficacy of GMS-VINS in segmentation within complex environments.

between anticipated and actual trajectory. In certain instances, this could result in a malfunction of the robot’s positioning system. Accordingly, solutions designed to reduce the influence of dynamic objects on estimation results is critical. Methods based on motion prior to eliminating the influence of dynamic objects [2]–[6] have been widely employed for the processing of dynamic objects; however, these methods remain inadequate for highly dynamic scenes. To overcome the shortcomings of methods based on motion prior, researchers have integrated semantic information to enhance performance of VIO systems in dynamic environments. Recent advancements [7]–[9] illustrate the effectiveness of semantic segmentation in enhancing resilience and accuracy, particularly in managing highly dynamic scenes in complex environments.

However, these methods primarily focus on specific dynamic objects and often overlook the generalizability of the segmentation model in environments with diverse moving objects (fig. 1). Earlier studies on dynamic VIO solution using traditional models like SegNet [10] and Mask R-CNN [11] were constrained by their limited capacity to segment multi-category dynamic objects. Partial occlusion of various moving objects in complex environments leads to a significant reduction in segmentation accuracy. As a result, while effective in certain scenarios, previous approaches lose reliability and pre-

*Corresponding author: jingbin.liu@whu.edu.cn

cision when environmental conditions change or new dynamic objects appear, thereby restricting their real-world applicability [12].

This work introduces GMS-VINS (Generalized Multi-Category Segmentation Visual-Inertial Navigation System), a universally applicable VIO method designed for dynamic environments involving diverse moving objects, incorporating an innovative multi-category segmentation technique. Our approach leverages the powerful zero-shot generalization capability of the Segment Anything Model (SAM) [13] for multi-category segmentation tasks. Furthermore, this strategy eliminates the necessity for explicit retraining for specific cases, enhancing GMS-VINS's adaptability to various dynamic environments. Furthermore, we have developed an enhanced SORT (Simple Online and Real-Time Tracking) [14] algorithm to improve the robustness of the target tracking model in complex urban environments, especially in cases of partial obstructions (fig. 1). We carried out extensive experiments on multiple datasets and real-world scenarios to assess the effectiveness of GMS-VINS in mitigating the influence of diverse dynamic objects in various environments. The experimental findings demonstrate that our proposed approach exhibits superior performance across a variety of scenarios, surpassing other state-of-the-art methods. This underscores its exceptional generalization and adaptability in different dynamic environments, highlighting its potential for managing diverse dynamic objects in real-world applications. Our main contributions are summarized as follows:

- We introduce an innovative VIO solution, GMS-VINS, designed for challenging dynamic conditions that exhibit exceptional adaptability and generalization in various environments.
- A new method is introduced to track and segment diverse dynamic objects using a promptable foundation model, aimed at mitigating performance degradation in VIO in dynamic environments.
- We proposed an enhanced SORT algorithm that efficiently maintains the tracking of moving objects under tough conditions with partial occlusion.
- Extensive experiments conducted on diverse public datasets and real-world scenarios demonstrate that GMS-VINS performs exceptionally well in varied environments, surpassing state-of-the-art methods in pose estimation accuracy.

II. RELATED WORKS

A. Visual-Inertial Odometry

Recently, Visual Inertial Odometry (VIO) have become a research focus in the fields of robotics applications. Based on the method of the fusion of visual and inertial measurements, classic VIO systems are generally classified into filter-based and optimization-based categories. Filter-based methods [15]–[19] typically utilize the extended Kalman filter (EKF) for pose estimation. Optimization-centric approaches [20]–[22],

[22]–[24] predominantly rely on the extraction of features and visual-inertial bundle adjustment to obtain precise pose estimation. Learning-based methods in VIO [25]–[28], have also been explored in recent years, yielding encouraging outcomes.

Integrating IMU motion data allows VIO systems to resist interference from moving objects in the background to some extent. Nevertheless, their performance in highly dynamic scenarios is still restricted. Specifically, when dynamic regions dominate the camera view, both the accuracy and reliability of VIO are greatly reduced, resulting in discrepancies between estimated and actual trajectories or even localization failure.

B. Dynamic Objects Removal in Visual and VI Odometry

It is crucial to develop solutions aimed at mitigating the impact of dynamic objects on the accuracy of VIO. In recent years, the use of visual methods to track dynamic objects has emerged as a prominent area of research. Fan et al. [2] and Sun et al. [6] put forth a multi-view geometry-based method that enhances RGB-D SLAM in dynamic environments. Tan et al. [3] presented a novel prior-based adaptive RANSAC algorithm (PARSAC) that effectively eliminates outliers, ensuring reliable camera pose estimation under dynamic conditions. Furthermore, some work is based on the structure of the plane, such as that presented in RP-VIO [5], which employs the simple geometry of planes to enhance robustness and accuracy in dynamic environments. RD-VIO [4] uses the IMU-PARSAC algorithm to robustly handle dynamic scenes. Most methods utilize motion priors from the IMU, allowing VIO to tolerate environments containing dynamic objects to some degree. However, when dynamic objects occlude a significant portion of the view, the issue cannot be solved solely by using the prior motion. [9]

In light of the advances of computer vision, researchers have integrated semantic information into VIO solutions aimed at addressing the constraints of approaches based on motion prior. Approaches such as DS-SLAM [7], DynaVINS [9], Mask-Fusion [29], Dynamic-VINS [8] and Dyna-SLAM [30] have integrated semantic segmentation methods, including SegNet [10] and Mask R-CNN [11], for the purpose of eliminating the effects of dynamic areas in the visual image.

Deep learning and pixel-level semantic segmentation yield significant outcomes in this area; however, they are restricted to the classes of segmented objects and conditions of partial occlusion. The limited generalizability of traditional segmentation models and their inadequacy in reducing the impact of moving objects with partial occlusions greatly impede their applicability in real-world scenarios. Although effective in specific environments, these methods suffer from accuracy and reliability under complex dynamic environmental conditions. Therefore, creating a universal segmentation technique to address these challenges for dynamic objects is essential for VIO applications in real-world situations.

C. Challenges in Multi-Category Semantic Segmentation

The intricacy of multi-category semantic segmentation is extensively recognized, with prior research [31]–[34] indicating considerable performance deterioration in models tasked with managing an array of diverse categories. When segmentation tasks extend across multiple datasets, they encounter persistent obstacles. These include inconsistencies in dataset taxonomies and integration difficulties, which frequently lead to degraded performance in tasks involving multi-category semantic segmentation [35]. A common problem in these tasks is the underperformance of tail classes, which is caused by compressed feature spaces resulting from an imbalanced data distribution [36]. In summary, segmenting multiple categories under diverse conditions remains a challenge. This issue is further exacerbated by the complexities of dataset diversity and data class distribution. Addressing these challenges by introducing a new method for multiple-category object semantic segmentation is crucial for real-world VIO applications, where high precision and adaptability across diverse environmental conditions are essential.

III. METHODOLOGY

This section details our methods for multi-category dynamic object segmentation and monocular VIO. We begin with the improved SORT algorithm and segmentation approach in section III-A, which is proficient in robust object segmentation across multiple categories in challenging environments. Subsequently, section III-B describes the feature tracking and compensation techniques in our VIO method.

A. Robust Tracking and Promptable semantic segmentation of multi-category dynamic objects

We present the improved SORT algorithm designed for stable tracking of potentially dynamic objects under partial occlusion conditions. Once the enhanced SORT algorithm is employed for tracking moving objects, the promptable foundation segmentation model is then used to identify moving components from static backgrounds at the pixel level.

Assuming that there are two adjacent frames $i - 1$ th and i th frame. Initially we utilize a tracking model to process these frames in the video sequences, generating a bounding box for every potential dynamic objects that detected by CNN. In order to ascertain which predicted box in the i th frame corresponds to a specific bounding box in the $i - 1$ th frame, we introduce the Hungarian algorithm to obtain the optimal estimate of the correspondence between multiple bounding boxes of objects in the images of the previous and subsequent frames. Once the correspondence of the bounding boxes has been established, the bounding box corresponding to any given box in a previous frame can be identified. Consequently, the Kalman filter [37] can be updated based on the previous state. For each bounding box, the state of the bounding box is defined as follows:

$$\hat{\mathbf{x}} = [x \quad y \quad w \quad h \quad v_x \quad v_y \quad v_w \quad v_h]^\top \quad (1)$$

In the state equation, the variables x and y represent the target center position, w and h represent the length and width of the bounding boxes, v_x and v_y represent the speed of movement of the target center position, v_w and v_h represent the time rate of change of the length and width of the bounding boxes.

Measurement noise covariance matrices \mathbf{R} are vital for the Kalman filter to accurately estimate dynamic states. Traditional methods for estimating these matrices are often inadequate for optimal filtering. [38] We propose an adaptive filtering method that dynamically estimates the measurement noise covariance matrix, \mathbf{R} , by analyzing residuals to enhance the Kalman filter's state estimation. This process utilizes a sliding window to collect residuals, computed using the function given below:

$$\delta_k = [\delta_x \quad \delta_y \quad \delta_w \quad \delta_h]_k = \mathbf{z}_k - \mathbf{H} \cdot \hat{\mathbf{x}}_{k|k-1} \quad (2)$$

Where $\delta_x, \delta_y, \delta_w, \delta_h$ represents the residuals vector, it quantifies discrepancies between the actual measurements \mathbf{z}_k and the predictions from the Kalman filter. \mathbf{H} represents the measurement matrix, which maps the predicted state $\hat{\mathbf{x}}_{k|k-1}$ to the measurement space. We calculate the δ_{RMSE} of the residuals in the sliding window of N frames, which provides a robust measure of the magnitude of the residuals, reflecting the average error magnitude over the sliding window, computed as :

$$\delta_{RMSE} = \left(\frac{1}{N} \sum_{i=1}^N (\delta_i)^2 \right)^{\frac{1}{2}} \quad (3)$$

This metric reflects the present variability in measurement noise, providing a real-time view of deviations from anticipated behavior. Once the RMSE values are acquired, the measurement noise covariance matrix \mathbf{R} is adaptively revised by applying a transformation to δ_{RMSE} . The measurement noise covariance matrix updating function is determined as

$$\mathbf{R} = \text{diag}(\beta \cdot \text{erf}(\lambda \cdot \delta_{RMSE})) \quad (4)$$

Where $\text{erf}(x)$ is the error function, which defined as:

$$\text{erf}(x) = \frac{2}{\sqrt{\pi}} \int_0^x e^{-t^2} dt \quad (5)$$

The parameters λ and β play pivotal roles in shaping the behavior of our function: λ modulates the steepness of the function's transition, while β determines the output's magnitude. The error function generates a smooth S-shaped curve that adeptly scales RMSE values, fostering stable and reliable filter behavior. Such smoothness is crucial for managing real-world data, particularly when dealing with outliers or noise, as it reduces the risk of the filter overreacting to these anomalies. Additionally, the function is designed to restrictively limit the impact of large residuals, thereby protecting against abrupt and significant alterations to \mathbf{R} . Utilizing a sliding window and error function scaling, this method adapts to measurement noise variations while maintaining estimation stability. It allows the Kalman filter to optimize performance

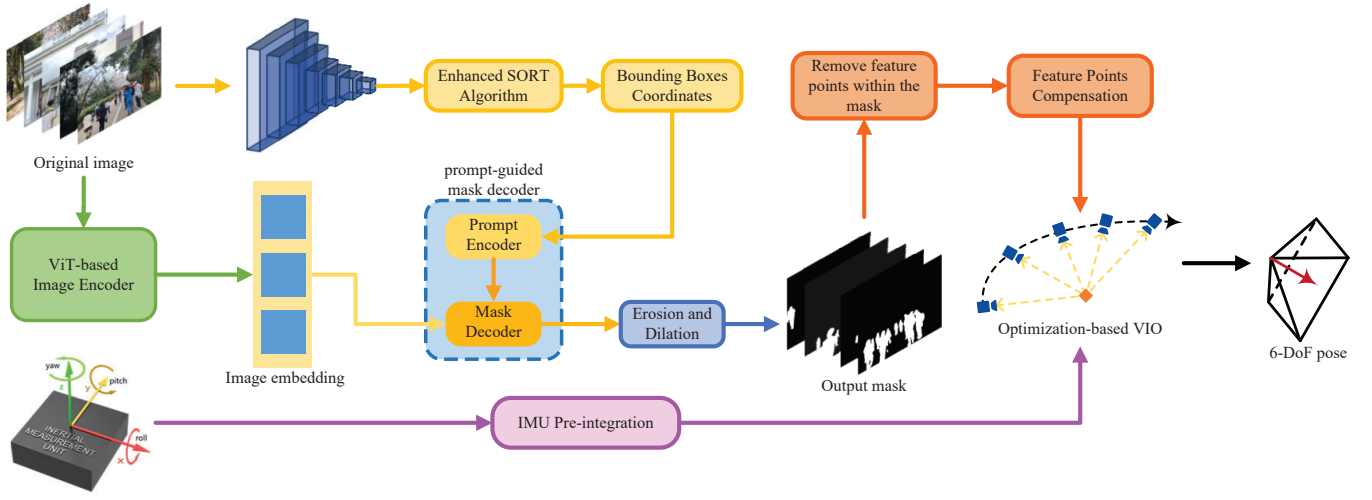


Fig. 2: Dynamical object segmentation based on object tracking pipeline

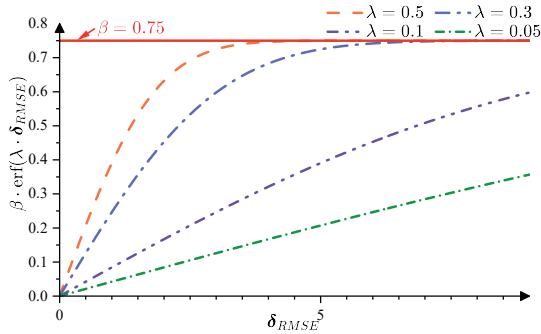


Fig. 3: Changes of measurement noise covariance matrix updating function w.r.t. parameter λ .

by adjusting parameters based on real-time accuracy and reliability, resulting in more precise state estimations under varying conditions. Subsequently, the predicted bounding boxes from adaptive Kalman filtering are used to rectify deficiencies in the original target detection model. This approach addresses multiple object tracking instability effectively, significantly enhancing the robustness and accuracy of dynamic object tracking in complex environments.

After the adaptive Kalman filtering method, The coordinates of these bounding boxes are then used to guide promptable foundation model in segmenting objects within the camera's field of view. In order to enhance the real-time performance of the method, we employ Mobile SAM as a promptable foundation model, which is more time-efficient and consumes fewer computational resources. Mobile SAM will perform segmentation focusing on the object that occupies the majority of the area delineated by these coordinates. This method ensures precise segmentation of moving objects tracked by the SORT algorithm, creating a mask that differentiates dynamic from static regions.

Furthermore, to enhance the mask quality, we further refine it through erosion and dilation processes. We opted for a

circular structure in processing the mask because it effectively preserves the original shape and details while minimizing the risk of distortion. The initial step involves denoising the mask using an erosion algorithm, which can effectively eliminates the small noise spots present in the mask. Assuming that the original mask is $\mathbf{M}_{original}$, the structure used for erosion is \mathbf{S}_{erode} and the eroded mask is \mathbf{M}_{erode} :

$$\begin{aligned} \mathbf{M}_{erode} &= \mathbf{M}_{original} \ominus \mathbf{S}_{erode} \\ &= \{x, y | (\mathbf{S}_{erode})_{xy} \subseteq \mathbf{M}_{original}\} \end{aligned} \quad (6)$$

The mask is further dilated to guarantee that the mask's dynamic region fully encompasses the object, preventing the extraction of feature points along the object's edges during feature extraction. Assuming the dilated mask \mathbf{M}_{dilate} and the dilation structure is \mathbf{S}_{dilate} . To eliminate the impact of mask reduction during erosion operations, one must ensure $\mathbf{S}_{dilate} > \mathbf{S}_{erode}$:

$$\begin{aligned} \mathbf{M}_{dilate} &= \mathbf{M}_{erode} \oplus \mathbf{S}_{dilate} \\ &= \{x, y | (\mathbf{S}_{dilate})_{xy} \cap \mathbf{M}_{erode} \neq \emptyset\} \end{aligned} \quad (7)$$

Through erosion and dilation processing, noise can be effectively eliminated, and the edges of dynamic regions can be covered without distorting the original mask, in preparation for feature point removal.

B. Robust feature tracking and optimization for VIO in dynamic scenes

The approach outlined in section III-A allows us to achieve semantic segmentation for dynamic objects, enabling us to filter out moving feature points based on segment masks. GMS-VINS employs KLT sparse optical flow [39] to track these feature points across frames. During this process, any points within the segmented area are tagged as dynamic and consequently discarded. New feature points are detected using the ORB algorithm [40] in the unmasked regions of the image.

Method	VIODE											
	City day				City night				Parking lot			
	none	low	mid	high	none	low	mid	high	none	low	mid	high
ORB-SLAM3 [23]	2.179	5.301	2.204	*	0.176	*	*	*	0.287	2.897	6.742	7.482
VINS-Fusion [22]	0.203	0.148	0.261	0.321	0.319	0.368	0.433	0.490	0.120	0.113	0.161	1.201
VINS-Mono [21]	0.186	0.237	0.263	3.169	0.314	0.436	0.727	0.575	0.102	0.109	2.915	4.933
RP-VIO [5]	0.382	0.229	0.435	0.536	0.263	0.509	0.652	0.577	0.981	1.334	0.375	0.713
Dyna-VINS [9]	0.349	0.330	0.258	0.245	0.687	0.207	0.251	0.311	0.046	0.106	0.118	0.107
GMS-VINS (Ours)	0.107	0.156	0.138	0.244	0.125	0.246	0.222	0.217	0.099	0.160	0.204	0.094

• *: Failure case.

TABLE I: Comparison with State-of-the-art Methods [5], [9], [21]–[23](RMSE of ATE in [M]). We highlight the top two results of each column in red and purple.

To ensure a robust distribution of feature points and keep a sufficient count of static points for precise pose estimation, we optimize feature point detection through Adaptive Non-maximal Suppression (ANMS) [41], which balances strength and spatial distribution of feature points. Additionally, a compensation strategy is applied to maintain an adequate number of feature points for precise pose estimation before bundle adjustment.

Denote \mathcal{K} as the set of ORB keypoints, with N_{max} as the maximum number of feature points and D_{min} as the minimum distance between them. Every feature point k_i is associated with a suppression radius ρ_i , expressed as:

$$\rho_i = \min\{\|\mathbf{p}_i - \mathbf{p}_j\| \mid r_j > r_i\} \quad (8)$$

where \mathbf{p}_i and \mathbf{p}_j are the positions of key points k_i and k_j , respectively, and r_i and r_j are their corresponding response values. Feature points are ranked by ρ_i in descending order, and the top N_{max} keypoints with the greatest suppression radius are selected. Subsequently, utilize D_{min} to filter feature points, ensuring that the spacing between two is not less than D_{min} . This method guarantees a consistent spatial distribution of high-quality features throughout the image.

Additionally, a compensation strategy is applied to maintain sufficient feature points for accurate pose estimation. The points tracked in the previous frame and the newly detected feature points in the m th frame are regarded as the set \mathcal{K}_m . The n th feature point is denoted as point k_m^n . The set of feature points detected in the $i - 1$ th frame can be expressed as:

$$\mathcal{K}_{i-1} = \{k_{i-1}^1, k_{i-1}^2, \dots, k_{i-1}^{n-1}, k_{i-1}^n\} \quad (9)$$

For optical flow matching between frame $i - 1$ and frame i , the points in \mathcal{K}_{i-1} that align in frame i are denoted as $j_i^1, j_i^2, \dots, j_i^s$. Given the altered positions of objects between the frames, we traverse the points $j_i^1, j_i^2, \dots, j_i^s$ to determine whether they fall within the mask's dynamic region; if they do, the points are excluded.

Assume that r points are excluded in this process, leaving $s - r$ points denoted as $j_i^1, j_i^2, \dots, j_i^{s-r-1}, j_i^{s-r}$, a new round of static feature point extraction should be performed in the i th frame. In this iteration of the feature point extraction

process, the maximum number of points to be extracted is set to $N_{max} - s + r$ for compensation. This guarantees that GMS-VINS has an adequate number of reliable static feature points for pose calculation, ensuring that the system can continue to operate stably even when the area of dynamic regions in the image is extensive. This enhances the robustness of GMS-VINS in complex dynamic environments. Suppose that r points are omitted during this procedure, resulting in $s - r$ points represented as $j_i^1, j_i^2, \dots, j_i^{s-r-1}, j_i^{s-r}$. In the newly i th frame, a fresh iteration of static feature point extraction is executed. During this iteration, the maximum number of extractable points is determined as $N_{max} - s + r$ to ensure compensation. This approach guarantees that GMS-VINS retains an adequate number of reliable static feature points for precise pose estimation, thus enabling the system to maintain stable operation even when a significant portion of the image is in motion.

IV. EXPERIMENTAL RESULT

A. Dataset

The VIODE [42] and OpenLORIS-Scene [43] datasets were selected for the evaluation of VIO solutions. VIODE [42] is a synthetic dataset captured from an aerial drone, containing sequences from three environments, with increasing complexity through four levels of dynamics. It is important to note that the subsequence nomenclature, ranging from 'none' to 'high,' denotes the dynamic level of the scene. The OpenLORIS-Scene dataset [43] includes a mix of visual, inertial, and odometric data from typical environments such as offices, homes, and commercial settings. It encompasses real-world challenges like changing lighting and moving individuals, closely resembling the everyday dynamic conditions. While VIODE centers on outdoor scenes with dynamic traffic scenarios, OpenLORIS encompasses various indoor scenes. These datasets were selected to evaluate the versatility of the VIO solution in different environmental conditions with varying dynamic objects.

B. Ablation Experiment for the Enhanced SORT algorithm

To assess the effectiveness of the improved SORT algorithm within GMS-VINS, we performed an ablation experiment

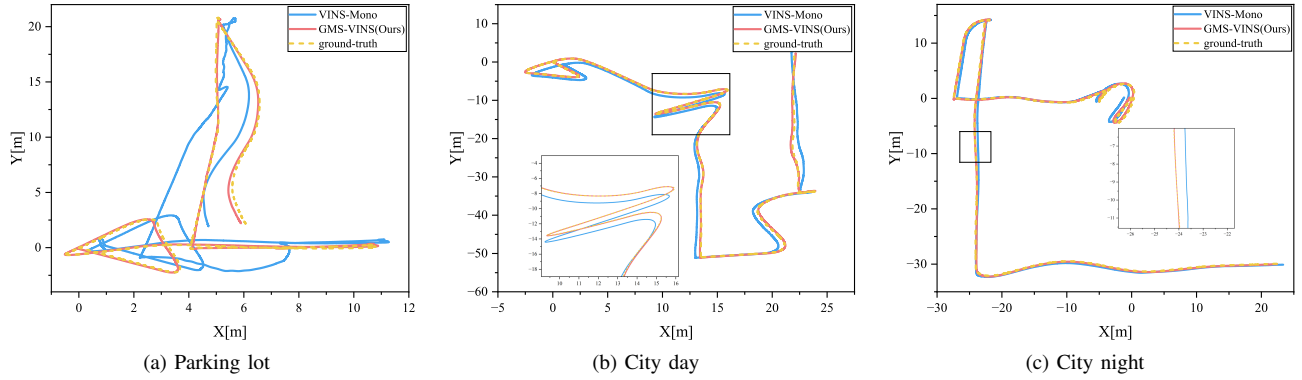


Fig. 4: A comparison of the trajectories of various VIO system on the "high" sequence of the VIODE dataset is presented. The ground truth is highlighted with a dashed yellow line. It can be observed that the trajectory obtained by GMS-VINS is the most accurate, with a high degree of overlap with the ground truth, reflecting the precision of the algorithm.

to examine its impact on GMS-VINS precision in dynamic environments.

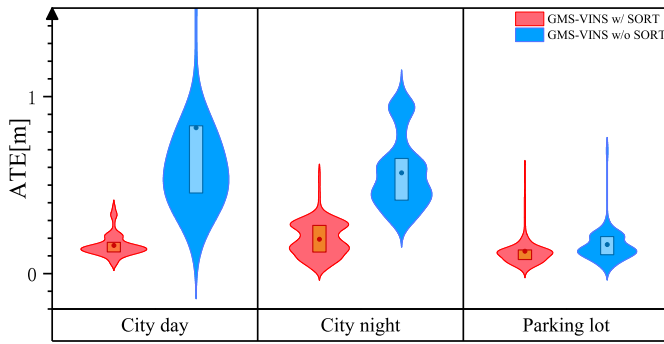


Fig. 5: Results of the ablation experiment for the enhanced SORT algorithm in GMS-VINS. This figure illustrates the ATE distribution for GMS-VINS in two configurations: including SORT (red) and excluding SORT (blue).

As demonstrated in fig. 5, the experimental data substantiates that the implementation of the SORT algorithm in the inertial visual odometry system notably enhances the positioning accuracy. In the parking lot scenario, the algorithm reduced the RMSE ATE by 21.38%. More substantial improvements were observed in urban settings, with an 83.28% reduction during daytime and a 63.99% reduction at night. These results indicate that our enhanced SORT algorithm significantly boosts GMS-VINS performance in challenging environments with a more effective state estimation approach. Particularly in scenarios with substantial alterations in illumination or occlusion relationships that result in inadequate visual data, the algorithm can effectively bolster the stability and precision of target tracking, minimize the deviations of inertial visual odometry, and reinforce the robustness and accuracy of the GMS-VINS system.

C. VIO Accuracy Evaluation on Public Dataset

To evaluate the enhancements of GMS-VINS in dynamic environments, we performed comparative experiments, employing the state-of-the-art approach VINS-Mono as the baseline for precision. We conducted experiments with various configurations of maximum feature points N_{max} and minimum feature point distance d_{min} in VIO to simulate different feature point densities. fig. 5 depict the outcomes. Our method demonstrates superior accuracy across various N_{max} and d_{min} configurations. The baseline's accuracy is severely impacted by N_{max} and d_{min} , lacking robustness and stability. Conversely, GMS-VINS demonstrates low RMSE ATE across the entire heatmap, indicating not only exceptional precision in dynamic pose estimation but also remarkable robustness and stability.

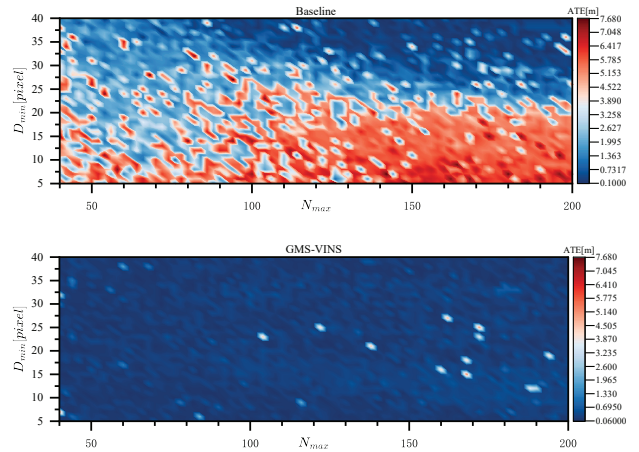


Fig. 6: The heatmap illustrates RMSE ATE in relation to the maximum feature points N_{max} and minimum feature point distance d_{min} for the "high" sequence within the parking lot environment of the VIODE dataset. The color bar represents the range of ATE values.

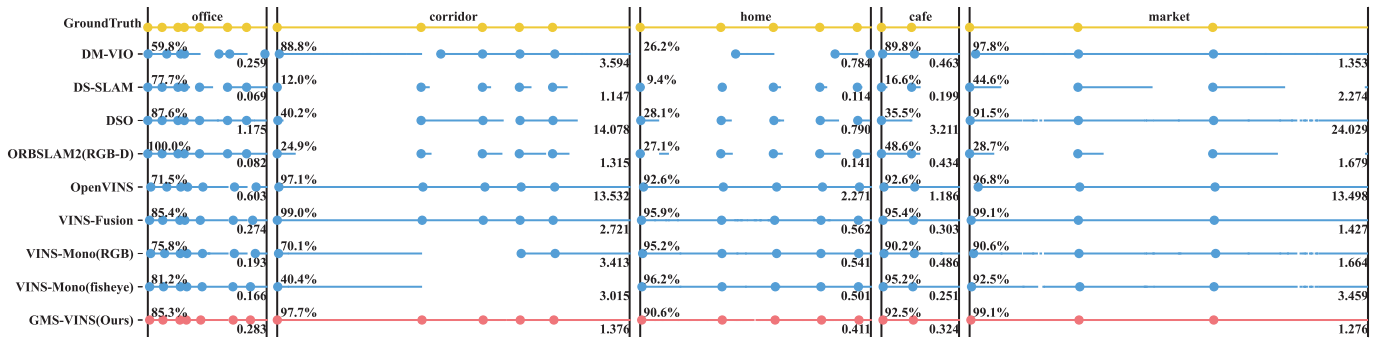


Fig. 7: Experiment results with the OpenLORIS-Scene datasets. For every algorithm, the dots represent successful initiation instances, and the lines show the span of successful tracking. The percentage in the top left corner of each scene indicates the average correct rate; a higher correct rate suggests greater algorithm robustness. The float value on the first line below depicts the average ATE RMSE, with lower values indicating higher accuracy. Some experimental results from prior methods are referenced from [43]

In our study, we conducted an evaluation of existing traditional Visual-Inertial Odometry (VIO) algorithms using the VIODE dataset. The outcomes of these evaluations are detailed in table I. Previous methods have proven effective in accurately estimating poses within static environments or in situations where there are only a few dynamic objects. However, as the prevalence of dynamic objects increases, particularly when they dominate the camera's field of view, the performance of these algorithms tends to decline markedly, resulting in notable deviations in trajectory calculations. In comparison to other methodologies, our proposed approach exhibits superior performance, especially in terms of RMSE of the absolute trajectory error (ATE) within the "high" sequence category of VIODE. It demonstrates comparable effectiveness to the DynaVINS in dynamic level sequences. Extensive analysis of the data suggests that the GMS-VINS algorithm is adept at navigating complex, dynamic traffic conditions and achieving considerable accuracy in trajectory estimations.

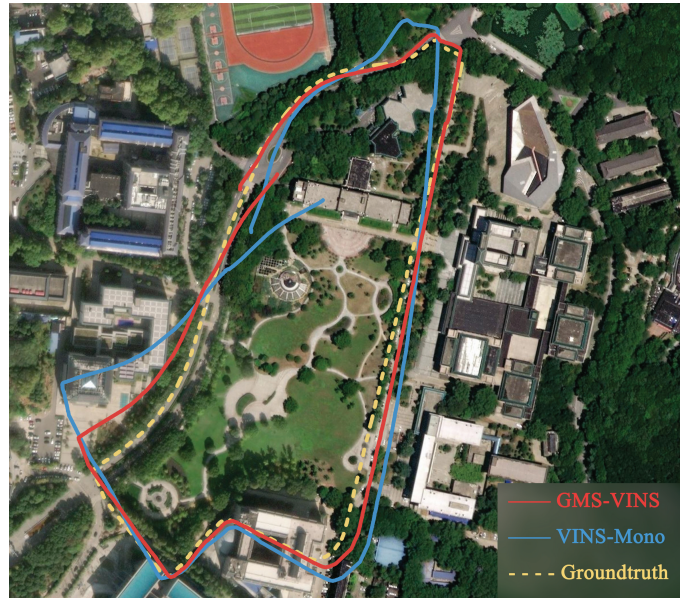


Fig. 9: The estimated trajectories in the real-world environment aligned with the satellite imagery from Microsoft. The red line is the estimated trajectory from GMS-VINS, the blue line is from VINS-Mono, and the yellow line represents the trajectory recorded from lidar-inertial odometry, which represents the ground-truth

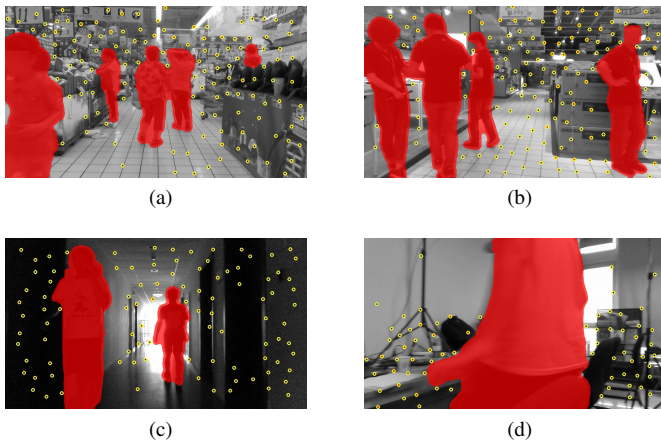


Fig. 8: The GMS-VINS performance across various OpenLORIS scenes.

To assess the generalizability of our approach, we conducted experiments using the challenging OpenLORIS dataset [43], which primarily features large-scale indoor scenes. Despite using RMSE ATE, the Correct Rate (CR) [43] is used as a metric to assess the robustness over the whole data period. The results of the experiment are depicted in fig. 7. Our approach drastically outperforms existing VIO techniques in market environments, superior in both RMSE ATE and accuracy rate. The market scenario (figs. 8a and 8b) in OpenLORIS features the highest variety and quantity of dynamic objects,

recorded in a supermarket full of people, shopping carts, and bags. These sequences present a tough obstacle for VIO’s ability to counteract the effects of dynamic objects. Consequently, GMS-VINS is demonstrated to be effective in challenging dynamic environments. In corridor scenes within the dataset, many methods struggle due to featureless walls and low-light conditions, which result in loss of tracking. However, due to the robust feature tracking and optimization detailed in section III-B, GMS-VINS exceeds other methods in terms of both accuracy and robustness, demonstrating its universality and adaptability in challenging environments. In other sequences, which contain fewer static objects and less challenging environments, GMS-VINS attains a competitive performance compared to state-of-the-art methods.

D. Experiment in real-world scenarios

In addition to validating our approach on public datasets, we also performed experiments in real-world settings. A RealSense D435i camera captures visual and inertial data for monocular visual-inertial SLAM. To provide ground-truth for the dataset, the robot equips a Mid-360 LiDAR to execute the FAST-LIO2 [44] algorithm for accurate trajectory acquisition. We collected an extensive outdoor dataset featuring a variety of moving objects, including pedestrians, cars, buses, motorcycles, and tricycles. Comprehensive details about the dataset are available in the appendix B. fig. 9 presents the alignment of the estimated and ground-truth trajectories with satellite images from Microsoft. In these complex environments, GMS-VINS demonstrated robust and stable pose estimation with minimal drift compared to the baseline method.

V. DISCUSSION AND CONCLUSION

This study presents GMS-VINS, an innovative VIO method that provides excellent accuracy in diverse and challenging dynamic environments. Unlike traditional semantic VIO method, GMS-VINS utilizing a promptable foundation model, overcomes limitations on segment-able objects and simplifies training complexity. We also developed an improved SORT algorithm by incorporating an adaptive Kalman filter, which enhances target tracking of moving objects under challenging circumstances with partial occlusion. Extensive experiments show that GMS-VINS effectively manages diverse dynamic objects, significantly enhancing accuracy in complex dynamic environments. Compared to state-of-the-art VIO methods, our approach improves trajectory accuracy, adapts to unseen scenarios, and offers a robust and efficient solution for advancing robotic systems.

However, Real-time semantic segmentation faces high computational demands and latency. Leveraging a remote server lightens the robot’s workload, enabling VIO to deliver precise pose estimates. In the future, we intend to further develop this methodology to improve the real-time performance of GMS-VINS by utilizing a remote server for practical real-world applications.

APPENDIX

A. Evaluation Metrics

In order to assess the precision of pose estimation, we employ Absolute Trajectory Error (ATE) [45] as a metric. Notably, as discussed in [43], the RMSE ATE is computed solely for its successful tracking results. However, failures in estimation are more severe than simple inaccuracies, especially within complex and dynamic environments featuring various moving objects. Consequently, we additionally utilize the Correct Rate (CR) as defined in [43] as an evaluation metric to further examine the robustness of the VIO method in the experiment described in section IV.

1) **Accuracy Metrics:** The Absolute Trajectory Error (ATE) [45] is utilized to evaluate the accuracy of the VIO system. Define $\mathbf{P}_1, \dots, \mathbf{P}_n \in SE(3)$ as the estimated trajectory of the VIO system and $\mathbf{Q}_1, \dots, \mathbf{Q}_n \in SE(3)$ as the ground-truth trajectory. The rigid body transformation matrix \mathbf{S} is derived by aligning the trajectory from $\mathbf{P}_1, \dots, \mathbf{P}_n \in SE(3)$ to $\mathbf{Q}_1, \dots, \mathbf{Q}_n \in SE(3)$ using optimized least squares. Consequently, the absolute trajectory error (ATE) at a given timestamp t_i is computed as follows:

$$ATE(\mathbf{P}_i) = \|\mathit{trans}(\mathbf{Q}_i^{-1}\mathbf{S}\mathbf{P}_i)\| \quad (10)$$

where $\mathit{trans}(\mathbf{Q}_i^{-1}\mathbf{S}\mathbf{P}_i)$ refers to the translational components of the pose error $\mathbf{Q}_i^{-1}\mathbf{S}\mathbf{P}_i$. We generally utilize the root mean square error (RMSE) of the Absolute Trajectory Error (ATE) across the full sequence as a criterion for assessing the precision of the VIO method applied to the sequence. The RMSE of ATE is defined as:

$$ATE(P_{1:n}, Q_{1:n}) = \left(\frac{1}{n} \sum_{i=1}^n ATE(\mathbf{P}_i)^2 \right)^{\frac{1}{2}} \quad (11)$$

RMSE ATE is efficient for precisely assessing the accuracy of the trajectory and pose estimations made by VIO, as it quantifies the deviation between the ground truth and the aligned estimated trajectory. The Absolute Orientation Error (AOE) can be calculated through comparable methods, primarily concentrating on the orientation error in pose estimation.

2) **Robustness Metrics:** To assess the robustness of VIO techniques, we utilize correctness and the correct rate (CR) as metrics. As referenced in [43], at each timestamp t_k , let $\mathbf{P}_k \in SE(3)$ denote the pose estimation produced by the VIO, and $\mathbf{Q}_k \in SE(3)$ denote the actual ground-truth pose. The parameters ε and ϕ are defined as the thresholds for Absolute Trajectory Error (ATE) and Absolute Orientation Error (AOE), respectively. The correctness of \mathbf{P}_k is specified as:

$$c^{\varepsilon, \phi}(\mathbf{P}_k) = \begin{cases} 1, & ATE(\mathbf{P}_k) \leq \varepsilon \text{ and } AOE(\mathbf{P}_k) \leq \phi \\ 0, & \text{otherwise} \end{cases} \quad (12)$$

While correctness assesses an individual pose estimate, for a sequence ranging from t_{min} to t_{max} , with an estimated

Sensor	Type	Specifications
Camera	Inter RealSense D435i	Sampling rate: 30Hz Resolution: 1280 × 720 RGB sensor FOV (H × V): 69° × 42°
LiDAR	Livox Mid-360	Sampling rate: 10Hz Operating range: 0.1 –70m
IMU	BMI085 (built-in D435i)	Measurement accuracy: ±3cm Sampling rate: 200Hz Resolution: Accelerometer: 0.1mg Gyroscope: 0.004°/s

TABLE II: Specifications of sensors employed in the real-world experiment.

trajectory $\{t_k, \mathbf{P}_k\}_{k=0, \dots, N}$, the Correct Rate (CR) can be formulated as:

$$CR^{\varepsilon, \phi} = \frac{\sum_{k=0}^N (\min(t_{k+1} - t_k, \delta) \cdot c^{\varepsilon, \phi}(\mathbf{P}_k))}{t_{\max} - t_{\min}} \quad (13)$$

where δ is a parameter used to ascertain the duration for which a correct pose estimation remains valid. In section IV, we employ CR^∞ , enabling a direct evaluation of the proportion of successfully completed pose predictions throughout the entire data time span. Employing CR^∞ provides a precise evaluation of the algorithm’s robustness, serving as a complementary measure to ATE, which only focuses on accuracy.

B. Detailed information of Real-World Experiment

In this section, we will provide comprehensive implementation details regarding the experiments conducted in real-world settings as described in section IV-D. To validate the efficacy of our proposed method, we conduct experiments utilizing data sourced from expansive and dynamic outdoor environments with a four-wheeled mobile robot, as depicted in fig. 10. Detailed specifications of sensors of the platform are provided in table II. For the purpose of enabling monocular visual-inertial odometry algorithms, we employed an Intel RealSense D435i camera integrated with a BMI085 IMU. The RealSense D435i camera is capable of capturing images at a resolution of 1280 × 720 pixels, ensuring high-quality imagery. Meanwhile, the integrated IMU functions at a sampling rate of 200 Hz, with its data hardware-synchronized to the captured images. The intrinsic and extrinsic parameters of the cameras and IMU of D435i are calibrated using Kalibr [46].

To offer reliable reference trajectories, the four-wheeled mobile robot is outfitted with a Mid360 LiDAR adjacent to the D435i camera. We utilized the FAST-LIO2 [44] algorithm on the LiDAR-collected data to produce highly accurate ground-truth poses as the ground-truth of the real-world experiments.

The sequence of the real-world experiment primarily encompasses complex urban traffic scenarios, which include a diverse array of dynamic elements, for instance, pedestrians, cars, buses, motorcycles, and tricycles. In such challenging dynamic environments, the ability of VIO methods to effectively manage various moving objects is of great importance. The experiment is capable of demonstrating the generalizability and adaptability of the VIO method when applied to real-world situations.



Fig. 10: Four-wheeled mobile robots equipped with sensors employed for conducting experiments in real-world environments.

REFERENCES

- [1] D. Nister, O. Naroditsky, and J. Bergen, “Visual odometry,” in *Proceedings of the 2004 IEEE Computer Society Conference on Computer Vision and Pattern Recognition, 2004. CVPR 2004.*, vol. 1, pp. I–I, 2004.
- [2] Y. Fan, H. Han, Y. Tang, and T. Zhi, “Dynamic objects elimination in slam based on image fusion,” *Pattern Recognition Letters*, vol. 127, pp. 191–201, 2019. *Advances in Visual Correspondence: Models, Algorithms and Applications (AVC-MAA)*.
- [3] W. Tan, H. Liu, Z. Dong, G. Zhang, and H. Bao, “Robust monocular

- slam in dynamic environments,” in *2013 IEEE International Symposium on Mixed and Augmented Reality (ISMAR)*, pp. 209–218, 2013.
- [4] J. Li, X. Pan, G. Huang, Z. Zhang, N. Wang, H. Bao, and G. Zhang, “Rd-vio: Robust visual-inertial odometry for mobile augmented reality in dynamic environments,” *IEEE transactions on visualization and computer graphics*, vol. 30, no. 10, pp. 6941–6955, 2024. Times Cited: 1 Huang, Gan/0000-0001-8515-2721; Li, Jinyu/0000-0002-5206-8600; Pan, Xiaokun/0000-0002-7438-1665; Zhang, Ziyang/0009-0004-4169-2282; Bao, Hujun/0000-0002-2662-0334; Zhang, Guofeng/0000-0001-5661-8430 0 1 1941-0506.
 - [5] K. Ram, C. Kharyal, S. S. Harithas, K. M. Krishna, and Ieee, “Rp-vio: Robust plane-based visual-inertial odometry for dynamic environments,” in *IEEE/RSJ International Conference on Intelligent Robots and Systems (IROS)*, IEEE International Conference on Intelligent Robots and Systems, pp. 9198–9205, 2021. Ram, Karnik Kharyal, Chaitanya Harithas, Sudarshan S. Krishna, K. Madhava Krishna, Madhava/JYO-4800-2024 2153-0858.
 - [6] Y. Sun, M. Liu, and M. Q. H. Meng, “Improving rgb-d slam in dynamic environments: A motion removal approach,” *Robotics and Autonomous Systems*, vol. 89, pp. 110–122, 2017. Times Cited: 250 Sun, Yuxiang/HPH-6656-2023; Meng, Max/C-8078-2009; Liu, Ming/AAC-9891-2020; Sun, Yuxiang/ Liu, Ming/ Sun, Yuxiang/0000-0002-7704-0559; Liu, Ming/0000-0002-4500-238X 1 279 1872-793x.
 - [7] C. Yu, Z. Liu, X.-J. Liu, F. Xie, Y. Yang, Q. Wei, and Q. Fei, “Ds-slam: A semantic visual slam towards dynamic environments,” in *25th IEEE/RSJ International Conference on Intelligent Robots and Systems (IROS)*, IEEE International Conference on Intelligent Robots and Systems, pp. 1168–1174, 2018. Times Cited: 489 Liu, Zuxin/GQY-8303-2022; Yu, Chao/HTS-5623-2023; Wei, Qi/JJF-3393-2023; Xie, Fugui/P-8259-2017; Liu, Zuxin/ Liu, Zuxin/0000-0001-7412-5074 2153-0858.
 - [8] J. Liu, X. Li, Y. Liu, and H. Chen, “Rgb-d inertial odometry for a resource-restricted robot in dynamic environments,” *Ieee Robotics and Automation Letters*, vol. 7, no. 4, pp. 9573–9580, 2022. Times Cited: 24 Liu, Jianheng/0000-0002-3124-5559; Liu, Yueqian/0000-0002-1994-6408 0 24.
 - [9] S. Song, H. Lim, A. J. Lee, and H. Myung, “Dynavins: A visual-inertial slam for dynamic environments,” *IEEE Robotics and Automation Letters*, vol. 7, no. 4, pp. 11523–11530, 2022.
 - [10] V. Badrinarayanan, A. Kendall, and R. Cipolla, “Segnet: A deep convolutional encoder-decoder architecture for image segmentation,” November 01, 2015 2015.
 - [11] K. He, G. Gkioxari, P. Dollár, and R. Girshick, “Mask r-cnn,” March 01, 2017 2017. open source; appendix on more results.
 - [12] J. X. Liu, M. L. Zeng, Y. C. Wang, and W. Liu, “Visual slam technology based on weakly supervised semantic segmentation in dynamic environment,” in *International Symposium on Artificial Intelligence and Robotics*, vol. 11574 of *Proceedings of SPIE*, 2020. Liu, Jianxin Zeng, Menglan Wang, Yuchao Liu, Wei LIU, jianxin/G-6396-2013 0277-786x 115740q.
 - [13] A. Kirillov, E. Mintun, N. Ravi, H. Z. Mao, C. Rolland, L. Gustafson, T. T. Xiao, S. Whitehead, A. C. Berg, W. Y. Lo, P. Dollár, R. Girshick, and Ieee, “Segment anything,” in *IEEE/CVF International Conference on Computer Vision (ICCV)*, IEEE International Conference on Computer Vision, pp. 3992–4003, 2023. Kirillov, Alexander Mintun, Eric Ravi, Nikhila Mao, Hanzi Rolland, Chloe Gustafson, Laura Xiao, Tete Whitehead, Spencer Berg, Alexander C. Lo, Wan-Yen Dollár, Piotr Girshick, Ross 1550-5499.
 - [14] A. Bewley, Z. Ge, L. Ott, F. Ramos, and B. Upcroft, “Simple online and realtime tracking,” in *2016 IEEE international conference on image processing (ICIP)*, pp. 3464–3468, IEEE, 2016.
 - [15] A. I. Mourikis, S. I. Roumeliotis, and Ieee, “A multi-state constraint kalman filter for vision-aided inertial navigation,” in *IEEE International Conference on Robotics and Automation ICRA*, pp. 3565–, 2007. Mourikis, Anastasios I. Roumeliotis, Stergios I. 1050-4729.
 - [16] M. Bloesch, S. Omani, M. Hutter, R. Siegwart, and Ieee, “Robust visual inertial odometry using a direct ekf-based approach,” in *IEEE/RSJ International Conference on Intelligent Robots and Systems (IROS)*, IEEE International Conference on Intelligent Robots and Systems, pp. 298–304, 2015. Times Cited: 554 Siegwart, Roland/A-4495-2008 Siegwart, Roland/0000-0002-2760-7983 2153-0858.
 - [17] M. Bloesch, M. Burri, S. Omari, M. Hutter, and R. Siegwart, “Iterated extended kalman filter based visual-inertial odometry using direct photometric feedback,” *International Journal of Robotics Research*, vol. 36, no. 10, pp. 1053–1072, 2017. Times Cited: 276 Siegwart, Roland/A-4495-2008 Siegwart, Roland/0000-0002-2760-7983 0 332 1741-3176.
 - [18] P. Geneva, K. Eickenhoff, W. Lee, Y. Yang, and G. Huang, “Openvins: A research platform for visual-inertial estimation,” in *2020 IEEE International Conference on Robotics and Automation (ICRA)*, pp. 4666–4672, 2020.
 - [19] Y. Fan, T. Zhao, and G. Wang, “Schurvins: Schur complement-based lightweight visual inertial navigation system,” December 01, 2023 2023. Accepted by CVPR2024.
 - [20] S. Leutenegger, S. Lynen, M. Bosse, R. Siegwart, and P. Furgale, “Keyframe-based visual-inertial odometry using nonlinear optimization,” *International Journal of Robotics Research*, vol. 34, no. 3, pp. 314–334, 2015. Leutenegger, Stefan Lynen, Simon Bosse, Michael Siegwart, Roland Furgale, Paul Bosse, Michael/B-7719-2011; Siegwart, Roland/A-4495-2008 Siegwart, Roland/0000-0002-2760-7983 1741-3176.
 - [21] T. Qin, P. Li, and S. Shen, “Vins-mono: A robust and versatile monocular visual-inertial state estimator,” *IEEE Transactions on Robotics*, vol. 34, no. 4, pp. 1004–1020, 2018.
 - [22] T. Qin, J. Pan, S. Cao, and S. Shen, “A general optimization-based framework for local odometry estimation with multiple sensors,” January 01, 2019 2019.
 - [23] C. Campos, R. Elvira, J. J. G. Rodríguez, J. M. M. Montiel, and J. D. Tardós, “Orb-slam3: An accurate open-source library for visual, visual-inertial, and multimap slam,” *IEEE Transactions on Robotics*, vol. 37, no. 6, pp. 1874–1890, 2021.
 - [24] L. Von Stumberg, V. Usenko, and D. Cremers, “Direct sparse visual-inertial odometry using dynamic marginalization,” in *2018 IEEE International Conference on Robotics and Automation (ICRA)*, pp. 2510–2517, 2018.
 - [25] W. Wang, Y. Hu, and S. Scherer, “Tartanvo: A generalizable learning-based vo,” in *Conference on Robot Learning*, pp. 1761–1772, PMLR, 2021.
 - [26] T. Zhou, M. Brown, N. Snavely, and D. G. Lowe, “Unsupervised learning of depth and ego-motion from video,” in *2017 IEEE Conference on Computer Vision and Pattern Recognition (CVPR)*, pp. 6612–6619, 2017.
 - [27] Y. Almalioğlu, M. Turan, M. R. U. Saputra, P. P. de Gusmão, A. Markham, and N. Trigoni, “Selfvio: Self-supervised deep monocular visual-inertial odometry and depth estimation,” *Neural Networks*, vol. 150, pp. 119–136, 2022.
 - [28] Y. Pan, W. Zhou, Y. Cao, and H. Zha, “Adaptive vio: Deep visual-inertial odometry with online continual learning,” in *Proceedings of the IEEE/CVF Conference on Computer Vision and Pattern Recognition (CVPR)*, pp. 18019–18028, June 2024.
 - [29] M. Runz, M. Buffier, and L. Agapito, “Maskfusion: Real-time recognition, tracking and reconstruction of multiple moving objects,” in *2018 IEEE International Symposium on Mixed and Augmented Reality (ISMAR)*, pp. 10–20, 2018.
 - [30] B. Bescos, J. M. Fàcil, J. Civera, and J. Neira, “Dynaslam: Tracking, mapping, and inpainting in dynamic scenes,” *IEEE Robotics and Automation Letters*, vol. 3, no. 4, pp. 4076–4083, 2018.
 - [31] G. Csürka and F. Perronnin, “An efficient approach to semantic segmentation,” *International Journal of Computer Vision*, vol. 95, pp. 198–212, 2011.
 - [32] J. Shen, L. Chen, K. Kuang, F. Wu, T. Feng, and W. Zhang, “Medoe: A multi-expert decoder and output ensemble framework for long-tailed semantic segmentation,” *ArXiv*, vol. abs/2308.08213, 2023.
 - [33] L. Yu, X. Liu, and J. van de Weijer, “Self-training for class-incremental semantic segmentation,” *IEEE Transactions on Neural Networks and Learning Systems*, vol. 34, pp. 9116–9127, 2020.
 - [34] R. Vieux, J. Benois-Pineau, J.-P. Domenger, and A. J.-P. Braquelaire, “Segmentation-based multi-class semantic object detection,” *Multimedia Tools and Applications*, vol. 60, pp. 305 – 326, 2010.
 - [35] Q. Zhou, Y. Liu, C. Yu, J. Li, Z. Wang, and F. Wang, “Lmseg: Language-guided multi-dataset segmentation,” *ArXiv*, vol. abs/2302.13495, 2023.
 - [36] Y. Wang, J. Fei, H. Wang, W. Li, T. Bao, L. Wu, R. Zhao, and Y. Shen, “Balancing logit variation for long-tailed semantic segmentation,” *2023 IEEE/CVF Conference on Computer Vision and Pattern Recognition (CVPR)*, pp. 19561–19573, 2023.
 - [37] R. E. Kalman, “A new approach to linear filtering and prediction problems,” *Journal of Basic Engineering*, vol. 82D, pp. 35–45, 1960.
 - [38] S. Akhlaghi, N. Zhou, and Z. Huang, “Adaptive adjustment of noise covariance in kalman filter for dynamic state estimation,” in *2017 IEEE Power & Energy Society General Meeting*, pp. 1–5, July 2017.

- [39] B. D. Lucas and T. Kanade, "An iterative image registration technique with an application to stereo vision," in *Proceedings of the 7th International Joint Conference on Artificial Intelligence - Volume 2, IJCAI'81*, (San Francisco, CA, USA), p. 674–679, Morgan Kaufmann Publishers Inc., 1981.
- [40] E. Rublee, V. Rabaud, K. Konolige, and G. Bradski, "Orb: An efficient alternative to sift or surf," in *2011 International Conference on Computer Vision*, pp. 2564–2571, 2011.
- [41] M. Brown, R. Szeliski, and S. Winder, "Multi-image matching using multi-scale oriented patches," in *2005 IEEE Computer Society Conference on Computer Vision and Pattern Recognition (CVPR'05)*, vol. 1, pp. 510–517 vol. 1, 2005.
- [42] K. Minoda, F. Schilling, V. Wüest, D. Floreano, and T. Yairi, "Viode: A simulated dataset to address the challenges of visual-inertial odometry in dynamic environments," *IEEE Robotics and Automation Letters*, vol. 6, no. 2, pp. 1343–1350, 2021.
- [43] X. Shi, D. Li, P. Zhao, Q. Tian, Y. Tian, Q. Long, C. Zhu, J. Song, F. Qiao, L. Song, Y. Guo, Z. Wang, Y. Zhang, B. Qin, W. Yang, F. Wang, R. H. M. Chan, and Q. She, "Are we ready for service robots? the openloris-scene datasets for lifelong slam," in *2020 IEEE International Conference on Robotics and Automation (ICRA)*, pp. 3139–3145, 2020.
- [44] W. Xu, Y. Cai, D. He, J. Lin, and F. Zhang, "Fast-lio2: Fast direct lidar-inertial odometry," *IEEE Transactions on Robotics*, vol. 38, no. 4, pp. 2053–2073, 2022.
- [45] J. Sturm, N. Engelhard, F. Endres, W. Burgard, and D. Cremers, "A benchmark for the evaluation of rgb-d slam systems," in *2012 IEEE/RSJ International Conference on Intelligent Robots and Systems*, pp. 573–580, 2012.
- [46] P. Furgale, J. Rehder, and R. Siegwart, "Unified temporal and spatial calibration for multi-sensor systems," in *2013 IEEE/RSJ International Conference on Intelligent Robots and Systems*, pp. 1280–1286, 2013.